NORSAR

NORSAR Scientific Report No. 1-2002

Semiannual Technical Summary

1 July - 31 December 2001

Frode Ringdal (ed.)

Kjeller, February 2002

6.2 Travel times and attenuation relations for regional phases in the Barents Sea region

This research is conducted under contract DTRA01-00-C-0107.

A database containing 42 events in the Barents Sea region has been compiled and analyzed with the aim of evaluating crustal models, travel times and attenuation relations in the context of performing regional detection threshold monitoring of this region. The 42 events are mostly located around the circumference of the study area due to the virtually aseismic nature of the Barents Sea itself. Regional P_n and S_n phases were observable for most events in the database, while P_g and L_g phases were only observable for events with ray paths within continental crust. This corroborates a number of previous observations of L_g-wave blockage across the Barents Sea. Three existing velocity models were evaluated, with a model having slightly lower S-velocities than earlier assumed in the upper mantle giving the overall best fit to the observed arrivals. In order to estimate magnitudes, short term average (STA) and spectral amplitude values were calculated in several frequency bands for all phase arrivals in the data base. There were no significant differences between spectral and STA amplitudes, so the latter were used as this parameter is more efficient to calculate in real-time processing. An inversion was performed in order to determine a P_n and S_n attenuation relation specific for this region. The resulting magnitudes based on P_n and S_n phases gave an internally consistent, reasonably stable set of values, which can be calibrated towards any existing global or regional scale. An attenuation relation was also determined for the L_g phase, but the low number of amplitude readings in this case renders the results less reliable.

Introduction

The Barents Sea region is an area which is of particular interest in the context of the comprehensive nuclear test ban treaty (CTBT), as it contains the former Soviet Union nuclear test sites on Novaya Zemlya. For this reason, it is of interest to perform regional seismic detection threshold monitoring in order to continuously assess the upper limit magnitude of events that could go undetected, and also to provide automatic locations for seismic events in the region with the best possible precision. The Threshold Monitoring (TM) method (e.g. Ringdal and Kværna, 1989; 1992; Kværna and Ringdal, 1999) uses continuous seismic data from a network of stations to calculate a threshold magnitude for each point in a grid, for which an event would have 90% probability of detection by the network. It is thus able to take varying noise levels, interfering signals from teleseismic events, data gaps, particularly favorable site-station transmission properties etc. into account, which traditional, static capability maps are incapable of doing (Ringdal and Kværna, 1992). However, for the threshold monitoring to be accurate, reliable travel time curves and attenuation relations are required for the target area. Ideally, calibration events should be available for all station/phase combinations at each target point. However, in practice, particularly in areas of low seismic activity such as the Barents Sea, it is necessary to rely on travel time curves calculated from a regional velocity model and regional attenuation relations. Still, a good coverage of seismic events is a requirement in order to determine mean regional values of such relations. In order to provide the necessary data for this region, we have compiled a database of recent events, and have attempted to extract the necessary information in spite of the less than optimal coverage.

Seismotectonic setting

The Barents Sea is an epicontinental sea, bordering on the Precambrian and Caledonian crust of northern Fennoscandia, the Kola Peninsula and northern Siberia to the south, and young passive margins to the north and west, formed during the Cenozoic opening of the Eurasian Basin and the Norwegian-Greenland Sea respectively (e.g. Faleide *et al.*, 1993). Large parts of the western margin and the oceanic crust to the west is covered by a huge sediment wedge deposited after the opening of the Norwegian-Greenland Sea, primarily during the Pliocene-Pleistocene age (Eidvin *et al*., 1993). The interior of the Barents Sea is underlain by large thicknesses of Upper Paleozoic to Cenozoic sediments, with accentuated Moho relief, leaving as little as ~4 km of crystalline basement under the deepest basins (Jackson *et al*., 1990; Faleide *et al.*, 1993).

The internal Barents Sea has very little seismic activity, implying a stable tectonic situation (Bungum and Lindholm, 1996). This has also been interpreted as a consequence of a relatively weak ridge-push force counteracted by tensional stresses related to Pliocene-Pleistocene erosional unloading (Fiedler and Faleide, 1996). The activity is significantly higher along the western Barents Sea margin, which is under weak oblique (NW-SE) compression from the north-Atlantic ridge, with the large Pliocene-Pleistocene sediment load likely being the most important stress-generating mechanism in these areas (Byrkjeland *et al*., 2000).

Northern Fennoscandia and the Kola Peninsula are areas of intermediate seismic activity, tending mainly toward earthquakes in the upper half of the crust. There appears to be some activity connected to a postglacial reverse and strike-slip fault system in northern Fennoscandia (Bungum and Lindholm, 1996), the stress tensor appears to have NW-SE compression approximately corresponding to the expected ridge-push direction (Hicks *et al*., 2000). There is also some seismic activity along the northern coast of the Kola Peninsula, while onshore northern Siberia has lower levels. The seismic activity in northern Fennoscandia is most likely tied to a combination of the tectonic ridge push force and constructive postglacial uplift stresses (Bungum and Lindholm, 1996). Novaya Zemlya and the Kara Sea to the east has some sporadic earthquake activity, as evidenced by some interesting events in recent years (e.g. Marshall *et al*., 1989; Ringdal *et al*., 1997; Bowers *et al*., 2001; Schweitzer and Kennett, 2002).

Database of seismic events

A total of 42 seismic events in the Barents Sea and northern Fennoscandia were used as the basis for this study. The events were selected to provide the best possible ray path coverage of the crust, although since large areas of the Barents Sea are in practice aseismic, there is a concentration of activity on the outer parts: Svalbard, western Barents Sea, northern Fennoscandia, the Kola Peninsula and Novaya Zemlya. The database consists of earthquakes, mining blasts and other explosions (both chemical and nuclear), and some events of unknown origin. Areas with large numbers of seismic events with similar locations were represented with a single event, in order to avoid introducing any bias towards these areas in the subsequent inversion.

In addition to waveform data from seismic array stations on mainland Norway (ARCES, NORES), we have also used available array data from Finland (FINES), Svalbard (SPITS), and the Russian Kola peninsula (APA). Data from the Amderma (AMD) station in northern Russia were available for 15 of the events, waveform data were also retrieved from the IRIS consortium for the Global Seismographic Network (GSN) seismic stations in Kevo, Northern Finland

(KEV), Lovozero on the Kola peninsula (LVZ) and Ny Ålesund on the Svalbard archipelago (KBS). The location of these nine stations used are shown along with the locations of the 42 selected seismic events in Fig. 6.2.1. The waveform data were re-analyzed, with emphasis placed on consistent phase identification and onset time picking of observable phases. Only phases that could be clearly observed and identified were analyzed and used. A preliminary relocation of the events was performed during the analysis, using the 'Fennoscandia' crustal model (Mykkeltveit and Ringdal, 1981) which is the model routinely used by NORSAR for seismic event location in northwestern Europe and the Barents Sea.

An investigation of which phases were observable on the different stations from various source areas was performed, in order to evaluate the geographical coverage for each phase. As expected, crustal phases (P_g and L_g) are in general only observable for paths that travel more or less exclusively within the shield areas, i.e. from onshore or coastal events in Fennoscandia and Svalbard. This confirms previous observations indicating the blockage of L_g phases that have paths crossing large sedimentary structures such as those encountered in the Barents Sea (e.g. Zhang and Lay, 1994; Baumgardt, 2001; Bowers *et al*., 2001). P_n and S_n phases are observable for most events with distances greater than 2-3 degrees. Fig. 6.2.2 shows phase maps for the ARCES array in northern Norway.

Crustal models and travel times

In order to be able to predict phase arrival times for a given origin in a threshold monitoring application, an accurate crustal velocity model is required. An evaluation of several available crustal models was therefore performed. Observed and theoretical travel times for two models are shown in Fig. 6.2.3, plotted according to epicentral distance after relocation with the corresponding model using HYPOSAT (Schweitzer, 2001). All depths were fixed at 10 km for this comparison. The Fennoscandia model (Mykkeltveit and Ringdal, 1981), shown in Table 6.2.1, gave a reasonably good travel time residuals, but there were some systematic discrepancies as clearly visible in Fig. 6.2.3. The L_g-phase arrivals have consistent and quite large negative residuals on average, while the S_n phases trend towards positive residuals. The P_n arrivals have quite large negative residuals, in particular around the 6 - 12 degree distance range. Two models from Schweitzer and Kennett (2002), named BAREY and BAREZ (Table 1) were also tested, with the BAREY model giving the lowest travel time residuals overall (Fig. 6.2.3). These two models were adapted from a model developed for the Barents and Kara Seas by Kremenetskaya *et al.* (2001) by making minor P-velocity adjustments and varying the P/S ratio in the upper mantle (Schweitzer and Kennett, 2002). The main differences between these two models are the S velocities in the upper mantle, which of course have the greatest effect on regional S phases propagating at these depths (S_n). The BAREY model has the lowest S velocities in the upper mantle while BAREZ has the highest. The Fennoscandia model has upper mantle S velocities between the other two models. As shown in Table 6.2.1, the velocity profiles for both P and S within the crust are virtually identical, with the Conrad discontinuity at 16 km and the Mohorovicic discontinuity at 40 km (Fennoscandia) and 41 km (BAREY/BAREZ) depth.

The small differences in upper mantle P velocities (Table 6.2.1) serve to reduce the observed P_n residuals after relocation. The resulting small differences in epicenter locations for the different models also have an effect on the travel times of crustal phases, most visible for the L_g onsets (Fig. 6.2.3). The BAREY model appears to be particularly accurate for paths from Novaya

Zemlya to Fennoscandia, which is the setting for which it was developed. The BAREZ model is slightly better for paths crossing the Barents Sea from Novaya Zemlya to the north-west (towards Svalbard and Bjørnøya), and also to the south (towards Amderma) (Schweitzer and Kennett, 2002). The BAREY model however provided the smallest overall travel time residuals for all paths in our data set. The geographic distribution of the travel time residuals for the Fennoscandia and BAREY models is shown in Fig. 6.2.4, showing the generally lower residuals, in particular for the S_n arrivals, obtained using the BAREY model.

Attenuation relations and magnitudes

In order to provide threshold magnitudes for a given location, it is essential to be able to convert observed amplitudes to event magnitudes at the target location. To this end an attenuation relation from Jenkins *et al.* (1998), based on Sereno (1990) is used:

$$M_L = \log A + \log\left(\left(\frac{\Delta}{200}\right)^{af+b}\right) \quad (1)$$

where A is amplitude in nanometers, Δ is the epicentral distance in km, f is the logarithmic center frequency of the passband at which the amplitude reading is taken, while a and b are phase-dependent constants. The value 200 represents a reference distance where the geometrical spreading changes from spherical to a more complicated function based on the phase analyzed (Sereno, 1990). Due to the fact that the decrease in seismic amplitude with epicentral distance is a combined effect of geometrical spreading, anelasticity and scattering, care must be taken in relating these coefficients to physical properties of the medium (cf. Alsaker *et al.*, 1991). However, this is not necessary for our purpose, as long as the relation as a whole is able to describe the amplitude/distance relation in a consistent and reasonably accurate manner. The relation was developed using spectral amplitudes, however for continuos processing it is more efficient to use time-domain short term average (STA) amplitudes. A comparison of STA amplitudes and spectral amplitudes in the same frequency bands for the selected events showed that they are in practice equivalent with regard to magnitude calculation ($A_{STA} \sim A_{SPEC}$). STA amplitudes were calculated in three frequency bands (2-4, 3-6 and 4-8 Hz) corresponding to three of the frequency ranges used in JENKINS *et al*. (1998), using a moving window with a step length of one sample and window lengths of 2 s length for P_n and 5 s for S_n and L_g. The maximum STA amplitude within 7.5 s (P_n), 10 s (S_n) and 15 s (L_g) after the observed phase onset was then selected. Only amplitude readings with a minimum signal-to-noise ratios (SNR) of 3.0 or greater for P_n and S_n and 2.5 or greater for L_g, compared to a noise window of 5 s length starting 10 s ahead of the observed onset time have been used. The SNR for L_g is almost always lower than for S_n or P_n, as the L_g phase arrives within the coda of the earlier onsets. Similarly, S_n arrivals generally show lower SNRs than P_n arrivals, although this can also depend on source effects and the relative noise situation at the seismic station.

Magnitudes calculated using equation (1) did reveal some inconsistencies between magnitudes calculated from different frequency bands, phases and stations, as shown in Fig. 6.2.5. The *a* and *b* coefficients used in this care were determined using data from eastern North America, central Asia and Australia by Jenkins *et al.* (1998) (Table 6.2.2), also applied by Bowers *et al.* (2001) for the Barents Sea. For ARCES it is clear that magnitudes calculated from STA values in the 2-4 Hz passband are systematically higher, by about 0.3 magnitude units on average, than magnitudes calculated in the 3-6 Hz passband, which again are almost 0.2 magnitude units

higher on average than magnitudes calculated from the 4-8 Hz passband. Similar discrepancies were observed at the other stations. As Fig. 6.2.5 also shows, there is a quite large, systematic offset between the P_n and S_n phase magnitudes calculated within the same frequency band at the same station. In addition, there are large discrepancies between magnitudes calculated from the same phase/frequency range at different stations. This implies that the relation does not accurately represent the attenuation of seismic waves for this set of reference events.

In order to provide an attenuation relation that better explains the measured amplitudes in the database, and also to determine station corrections for the nine stations used, an inversion of the available amplitude data was performed. Using equation (1), the STA amplitude A_{ijk} for phase i from event j measured at station k may be expressed as:

$$a_i f \log\frac{\Delta}{200} + b_i \log\frac{\Delta}{200} + S_{ik} - M_j = -\log A_{ijk} \tag{2}$$

where S_{ik} is the station correction for phase i at station k, and M_j is the event magnitude for event j. The parameters a_i and b_i are the coefficients from equation (1) for phase i. Equation (2) represents a set of linear equations, and can be written in matrix form:

$$Ax = D \tag{3}$$

where A represents the Jacobi matrix, x the vector of unknowns and D is the data vector. We used standard, least-squares techniques to solve equation (2).

A total of 863 amplitude readings with acceptable SNR (≥3.0) from P_n (548 readings) and S_n (315 readings) phases from the 40 seismic events that had sufficient data to be used, were inverted in order to yield the two relation coefficients and nine station corrections for each of the two phases, in addition to relative magnitudes for the 40 events. The individual events had between four and 40 amplitude readings contributing to the solution. The a_i and b_i values determined through this inversion are given in Table 6.2.2, while the corresponding station corrections S_{ik} are listed in Table 6.2.3. New magnitudes calculated using these results are plotted in Fig. 6.2.6, showing that the mean offset was reduced in all cases compared to the original calculations (Fig. 6.2.5). The scatter, expressed as the standard deviation, was marginally higher for some combinations, and reduced for others.

The magnitudes for the P_n and S_n phases calculated using the inversion results are internally consistent, and can thus be tied in to any other magnitude scale. To calibrate the scale in this case we have used five events in the Novaya Zemlya region with body wave magnitudes ranging from m_b 2.4 to 5.6 (Table 4) that have previously been studied in great detail (e.g. Ringdal and Kremenetskaya, 1999), giving a constant offset of -0.33. Applying this offset value and the estimated phase-dependant station corrections S_i (listed in Table 6.2.3) to equation (1), the final magnitude relation for P_n and S_n STA amplitudes yields:

$$M_{L(P_n, S_n)} = \log A + \log\left(\left(\frac{\Delta}{200}\right)^{a_i f + b_i}\right) + S_i - 0.33 \tag{4}$$

where A is observed STA amplitude within a frequency band with logarithmic center frequency f, Δ is epicentral distance, and a_i and b_i are phase-dependant constants given in Table 6.2.2. The

P_n and S_n magnitudes calculated using equation (4) were in general comparable to previously reported magnitudes for other, well studied events, as shown in Table 6.2.4.

A separate inversion was attempted in order to determine coefficients for the L_g phase for events and stations located within Fennoscandia, as L_g observations are limited to this area. The inversion gave seemingly acceptable results when applied to our small group of events, however, attenuation was extremely low for distances over around 500 km. Given this contrast to the general M_L relation for Norway from Alsaker *et al*. (1991), the inversion in this case appears to be unable to adequately constrain the required parameters. Data from more event/ station combinations in Fennoscandia are needed in order to provide a valid L_g STA-based magnitude relation for Fennoscandia. L_g magnitude relations are anyhow of little interest with regard to magnitude estimation for events in the Barents and Kara Seas due to the strong attenuation or blocking of L_g energy observed for events in this area.

Fig. 6.2.7 shows comparisons of corrected network magnitudes as calculated from individual phases. There are still clear discrepancies between P_n and S_n magnitudes for different source areas, which seem to be the result of different ray paths. Events that predominantly have ray paths within Fennoscandia have larger S_n magnitudes (relative to P_n), while the opposite is true for events that have ray paths crossing the sediment basins of the Barents Sea (Novaya Zemlya/ Kara Sea and the western Barents Sea/Mid-Atlantic ridge areas). Table 4 lists the date, location and P_n, S_n, and overall network magnitudes with number of readings and RMS values for the 42 events in the database. Magnitudes (M_L) estimated by NORSARs GBF system (Ringdal & Kværna, 1989) and reference magnitudes (m_b) for the five Novaya Zemlya events from Ringdal and Kremenetskaya (1999) are also given.

Data from the Amderma station

The seismic station in Amderma (AMD) has a unique and important location with regard to studying seismic activity in the eastern Barents Sea/Kara Sea area (Fig. 6.2.1). Data from this station have not been generally available, but waveform data for a number of events in the Barents Sea region were collected as part of a joint project between NORSAR and the the Kola Regional Seismological Centre in Apatity. These data covered a total of 15 of the 42 events in our database, of which phase arrivals could be identified for 13 of the events. These arrivals represent an important contribution to the evaluation of the models. The epicentral distances for the majority of the events in the database are larger than for the other stations used in this study, so only nine events had onsets with SNRs large enough to be included in the inversion of the attenuation relations. Magnitudes calculated from amplitude observations at AMD using the coefficients determined by the magnitude inversion in this study appear to correlate on average quite well to the other stations, although the scatter is somewhat higher. The higher scatter is most likely an effect of the significantly different location (and thereby differences in ray paths), and also the relatively low number of good amplitude readings for this station compared to the other stations used in this study.

Conclusions

The following main conclusions can be drawn from this study of regional phases in the Barents Sea region:

The pattern of L_g arrivals and associated amplitudes support the previously published indications that the deep sediment basins and Moho topography under the Barents Sea efficiently blocks L_g wave energy from crossing.

The 'BAREY' model (Table 6.2.1) from Schweitzer and Kennett (2002), based on a model for the Barents Sea area from Kremenetskaya *et al.* (2001), provides the smallest overall travel time residuals when locating events within the vicinity of the Barents- and Kara Seas.

The attenuation in the Barents Sea region differs somewhat from that observed in other stable tectonic regions, as evidenced by the fact that the coefficients given by Jenkins *et al*. (1998) for such regions do not give consistent magnitudes across frequencies, phases and stations for our amplitude observations from the events in the Barents Sea region.

Amplitude inversion has been used in this study to resolve new coefficients and station corrections for estimating M_L magnitudes from STA amplitude observations for P_n and S_n phases in the Barents Sea region (Tables 6.2.2 and 6.2.3). The number of L_g amplitude observations for raypaths within northern Fennoscandia was too low to provide a usable magnitude relation for L_g. A future study using a greater number of continental events could most likely provide a more stable relation for STA based L_g magnitudes.

The magnitudes determined using the relation in equation (4) are self-consistent, and can be tied in to any other global, regional or local magnitude scale. The relation given in equation (4) has been adjusted in order to comply with body wave magnitudes for five events at Novaya Zemlya from Ringdal and Kremenetskaya (1999).

The seismic station in Amderma can be tied in to the regional network in Fennoscandia and on the Svalbard archipelago using an appropriate crustal model, and is able to provide important information regarding the location of events in the eastern parts of the Barents Sea and the Kara Sea (Schweitzer and Kennett, 2002). Magnitudes calculated at this station are on the whole quite consistent with the other observations.

The BAREY velocity model (Schweitzer and Kennett, 2002), and attenuation relation given in equation (4), currently provide the best possible locations and magnitudes for events in the Barents Sea region, and can be used for a Threshold Monitoring implementation for this area. When more and better quality data become available it may be possible to further improve these results, although the aseismic nature of the Barents Sea will continue to pose problems with regard to a detailed study of seismic wave propagation within the Barents Sea itself.

E.C. Hicks
T. Kværna
S. Mykkeltveit
J. Schweitzer
F. Ringdal

References

Alsaker, A., Kvamme, L.B., Hansen, R.A., Dahle, A. and Bungum, H. (1991): *The M_L scale in Norway,* Bull. Seis. Soc. Am *81,* 379-398.

Baumgardt, D.R. (2001), *Sedimentary basins and the blockage of Lg wave propagation in the continents*, Pure Appl. Geophys. *158*, 1207-1250.

Bowers, D., Marshall, P.D., and Douglas, A. (2001): *The level of deterrence provided by data from the SPITS seismometer array to possible violations of the Comprehensive Test Ban in the Novaya Zemlya region*, Geophys. Jour. Int. *146*, 425-438.

Bungum, H., and Lindholm, C. (1996), *Seismo- and neotectonics in Finnmark, Kola and the southern Barents Sea part 2: Seismological analysis and seismotectonics*, Tectonophys. *270*, 15-28.

Byrkjeland, U., Bungum, H., and Eldholm, O. (2000), *Seismotectonics of the Norwegian continental margin*, Jour. Geophys. Res. *105*, 6221-6236.

Eidvin, T., Jansen, E., and Riis, F. (1993), *Chronology of Tertiary fan deposits off the western Barents Sea: Implications for the uplift and erosion history of the Barents Shelf*, Mar. Geol. *122*, 19-131.

Fiedler, A., and Faleide, J.I. (1996), *Cenozoic sedimentation along the southwestern Barents Sea margin in relation to uplift and erosion of the shelf*, Global Planet. Change *318*, 75-93.

Faleide, J.I., Vågnes, E., and Gudlaugsson, S.T. (1993), *Late Mesozoic-Cenozoic evolution of the south-western Barents Sea in a regional rift-shear tectonic setting*, Mar. Petrol. Geol. *10*, 186-214.

Hicks, E.C., Bungum, H., and Lindholm, C.D. (2000), *Stress inversion of earthquake focal mechanism solutions from onshore and offshore Norway,* Nor. Geol. Tidsskr. *80*, 235-250.

Jackson, H.R., Faleide, J.I., and Eldholm, O. (1990), *Crustal structure of the sheared southwestern Barents Sea margin*, Mar. Geol. *93*, 119-146.

Jenkins, R.D., Sereno, T.J., and Brumbaugh, D.A. (1998), *Regional attenuation at PIDC stations and the transportability of the S/P discriminant* (AFRL-VS-HA-TR-98-0046, Science Applications International Corporation, San Diego, Ca, USA).

Kværna, T., and Ringdal, F. (1999), *Seismic threshold monitoring for continuous assessment of global detection capability,* Bull. Seis. Soc. Am. *89*, 946-959.

Kremenetskaya, E., Asming, V., and Ringdal, F. (2001). *Seismic location calibration of the European Arctic,* Pure Appl. Geophys. *158,* 117-128.

Marshall, P.D., Stewart, R.C., and Lilwall, R.C. (1989), *The seismic disturbance on 1986 August 1 near Novaya Zemlya: A source of concern?* Geophys. Jour. Int. *98*, 565-573.

Mykkeltveit, S., and Ringdal, F. (1981), *Phase identification and event location at regional distance using small-apature array data*, In *Identification of seismic sources - Earthquake or underground explosions* (eds. Husebye, E.S. and Mykkeltveit, S.), pp. 467-481.

Ringdal, F., and Kremenetskaya, E. (1999), *Observed characteristics of regional phases and implications for P/S discrimination in the Barents/Kara Sea region*, In: *NORSAR Sci. Rep. 2-98/99*, Kjeller, Norway.

Ringdal, F., and Kværna, T. (1989), *A multi-channel processing approach to real time network detection, phase association, and threshold monitoring*, Bull. Seis. Soc. Am. *79*, 1927-1940.

Ringdal, F., and Kværna, T. (1992), *Continuous seismic threshold monitoring*, Geophys. J. Int. *111*, 505-514.

Ringdal, F., Kværna, T., Kremenetskaya, E., and Asming, V. (1997), *The seismic event near Novaya Zemlya on 16 August 1997*. Semiannual Technical Summary, 1 April-30 September 1997, NORSAR Sci. Rep. 1-97/98, Kjeller, Norway.

Schweitzer, J. (2001), *HYPOSAT - An enhanced routine to locate seismic events*, Pure Appl. Geophys. 158, 277-289.

Schweitzer, J., and Kennett, B.L.N. (2002), *Location studies for the Kara Sea event 16 August 1997*, Semiannual Technical Summary, 1 July - 31 December 2001, NORSAR Sci. Rep. 2-2001/2002, Kjeller, Norway.

Sereno, T.J. (1990), *Attenuation of regional seismic phases in Fennoscandia and estimates of arrival time and azimuth uncertainty using data recorded by regional arrays*, Tech. Rep. SAIC-90/1472, Science Applications International Corp.

Zhang, T., and Lay, T. (1994), *Effects of crustal structure under the Barents and Kara seas on short-period regional wave propagation for Novaya Zemlya explosions: empirical relations*, Bull. Seis. Soc. Am. *84*, 1132-1147.

Fennoscandia			BAREY			BAREZ		
Depth (km)	**V_P**	**V_S**	**Depth (km)**	**V_P**	**V_S**	**Depth (km)**	**V_P**	**V_S**
0.0	6.20	3.58	0.0	6.20	3.58	0.0	6.20	3.58
16.0	6.20	3.58	16.0	6.20	3.58	16.0	6.20	3.58
16.0	6.70	3.87	16.0	6.70	3.87	16.0	6.70	3.87
40.0	6.70	3.87	41.0	6.70	3.87	41.0	6.70	3.87
40.0	8.15	4.705	41.0	8.10	4.58	41.0	8.10	4.71
			70.0	8.23	4.65	70.0	8.23	4.78
95.0	8.15	4.705						
95.0	8.25	4.763						
210.0	8.30	4.792	210.0	8.26	4.67	210.0	8.26	4.80

Table 6.2.1. The Fennoscandia (Mykkeltveit and Ringdal, 1981), BAREY and BAREZ (Schweitzer and Kennett, 2002) crustal models. The main differences between the models are the slightly different velocities in the uppermost mantle.

	P_n		**S_n**	
	a	**b**	**a**	**b**
JENKINS *et al.* (1998)	0.08	1.44	0.12	1.85
This study	0.36±0.02	0.88±0.09	0.41±0.02	0.63±0.11

Table 6.2.2. The inversion results for the a and b coefficients (±1σ) for P_n and S_n phases used in the attenuation relation (equations 4). The values from Jenkins et al. (1998) are shown for comparison. Note that the new coefficients have a stronger frequency dependency (higher a values).

Station	P_n	S_n
AMD	0.05±0.07	0.01±0.07
APA	0.15±0.04	-0.16±0.05
ARCES	0.13±0.04	0.03±0.04
FINES	0.13±0.05	-0.01±0.05
KBS	-0.07±0.04	-0.02±0.07
KEV	-0.09±0.04	-0.37±0.05
LVZ	0.09±0.04	-0.29±0.05
NORES	0.13±0.05	0.09±0.07
SPITS	0.05±0.04	0.12±0.09

Table 6.2.3. .Station corrections (±1σ) in magnitude units obtained as part of the inversion.

Date/time	Lat.	Lon.	P_n (M_L)			S_n (M_L)			Network (M_L)			GBF (M_L)		Ref.
			Mag.	no	RMS	Mag.	no	RMS	Mag.	no	RMS	Mag.	no	(m_b)
1988-235:16.20.00.13	*66.64*	*79.38*	*5.10*	*1*	-	-	-	-	5.1	1	-	-	-	
1990-167:12.43.26.91	68.95	34.62	3.75	2	0.30	3.98	2	0.27	3.86	4	0.31	-	-	
1990-297:14.58.06.49	72.50	54.08	5.65	1	-	5.16	1	-	5.41	2	0.25	-	-	5.6
1991-157:12.46.11.32	65.57	22.88	3.18	2	0.20	3.41	2	0.12	3.29	4	0.20	-	-	
1991-236:10.56.29.65	65.73	31.69	3.48	1	-	3.65	1	-	3.57	2	0.09	-	-	
1992-366:09.29.25.84	73.77	54.24	3.02	1	-	2.71	1	-	2.87	2	0.16	2.25	1	2.7
1993-005:10.19.34.40	64.68	17.29	3.97	4	0.26	4.16	3	0.22	4.05	7	0.26	3.61	7	
1995-013:04.34.08.58	75.95	8.90	3.45	8	0.29	3.44	3	0.07	3.45	11	0.25	-	-	
1995-021:01.58.07.21	70.43	18.39	2.99	5	0.08	3.34	4	0.18	3.14	9	0.22	2.99	10	
1995-054:21.50.00.15	71.19	54.53	2.18	2	0.16	2.34	1	-	2.23	3	0.15	-	-	
1995-063:18.29.04.36	82.25	28.71	3.65	6	0.17	3.65	5	0.21	3.65	11	0.19	3.10	1	
1995-101:20.07.23.02	80.05	35.67	3.67	5	0.18	3.83	4	0.22	3.75	9	0.22	3.25	2	
1995-102:08.18.52.49	69.26	33.38	2.35	4	0.25	2.54	1	-	2.39	5	0.24	2.04	5	
1995-133:22.38.51.04	76.89	9.54	3.54	9	0.15	3.46	4	0.11	3.51	13	0.14	3.13	3	
1995-161:18.45.34.11	75.70	33.88	2.55	3	0.10	2.56	3	0.14	2.56	6	0.12	2.01	2	
1995-162:19.27.15.07	*75.65*	*33.78*	*3.29*	*3*	*0.18*	*3.33*	*2*	*0.27*	3.31	5	0.22	*2.93*	*2*	
1995-164:19.22.38.41	75.10	56.02	3.51	4	0.22	3.53	5	0.21	3.52	9	0.21	2.74	2	3.5
1995-184:12.49.32.76	69.64	25.07	2.90	3	0.13	3.21	1	-	2.98	4	0.17	2.94	9	
1995-185:03.26.24.87	79.94	94.76	3.71	2	0.13	3.73	3	0.06	3.72	5	0.10	3.15	1	
1995-241:22.12.19.06	77.14	22.33	3.75	4	0.12	3.53	2	0.09	3.67	6	0.15	3.54	3	
1995-261:03.26.06.18	66.51	30.64	2.86	6	0.19	3.14	2	0.05	2.93	8	0.20	2.96	11	
1995-313:01.10.23.59	66.73	33.51	2.91	6	0.08	3.06	3	0.08	2.96	9	0.11	3.12	11	
1995-329:19.41.26.68	77.17	18.14	3.65	6	0.35	3.72	5	0.05	3.68	11	0.26	3.50	5	
1996-013:17.17.23.57	75.02	56.02	2.46	2	0.16	2.42	2	0.24	2.44	4	0.20	1.90	2	2.4
1996-021:02.16.32.03	69.25	24.25	3.72	7	0.30	4.00	2	0.08	3.78	9	0.29	3.86	12	
1996-218:20.04.38.23	75.58	14.63	3.13	7	0.29	3.09	4	0.07	3.12	11	0.24	2.38	3	
1996-272:06.08.47.35	69.39	32.03	1.95	3	0.21	-	-	-	1.95	3	0.21	1.60	1	
1996-301:23.55.17.21	79.88	23.54	3.45	4	0.24	2.99	1	-	3.36	5	0.28	2.62	1	
1996-361:04.44.15.67	63.24	44.62	2.98	4	0.08	3.00	3	0.16	2.99	7	0.12	2.74	4	
1997-122:07.31.17.23	72.67	20.85	2.86	6	0.24	2.68	4	0.14	2.78	10	0.22	2.15	2	
1997-228:02.11.00.36	72.48	57.67	3.42	5	0.24	3.52	2	-	3.43	7	0.23	-	-	3.5
1997-279:12.33.27.04	76.44	24.01	3.77	4	0.07	3.83	3	0.15	3.8	7	0.12	3.27	5	
1997-279:21.17.31.53	73.84	10.78	3.26	5	0.18	2.75	1	-	3.17	6	0.25	2.96	2	
1997-279:21.29.18.26	73.38	7.42	3.83	4	0.11	3.41	1	-	3.75	5	0.20	2.95	5	
1999-229:04.44.37.19	67.85	34.15	3.99	6	0.25	3.90	3	0.08	3.96	9	0.22	3.90	13	
1999-290:12.07.16.70	70.43	18.64	3.55	7	0.20	3.90	1	-	3.59	8	0.22	3.79	13	
2000-225:07.30.41.31	69.66	37.38	3.41	8	0.35	3.14	3	0.03	3.34	11	0.32	2.80	8	
2000-316:02.01.06.65	75.35	16.76	3.52	6	0.33	3.93	4	0.22	3.68	10	0.35	3.46	4	
2000-341:00.34.40.15	76.17	8.77	3.86	3	0.14	3.27	1	-	3.71	4	0.29	2.94	4	
2000-360:03.50.28.47	73.32	14.01	3.68	8	0.19	3.64	5	0.14	3.66	13	0.18	3.39	9	
2001-090:11.30.55.35	66.41	13.67	3.90	8	0.25	4.16	6	0.10	4.01	14	0.24	4.00	13	
2001-122:15.59.43.93	67.23	24.70	2.93	5	0.07	3.20	2	0.05	2.97	12	0.12	3.07	10	

Table 6.2.4. Origin time and locations for the 42 seismic events after relocation using the BAREY model. Magnitudes (M_L) were calculated using the attenuation parameters determined through inversion, using amplitude observations in the 3-6 Hz frequency band. Mean magnitudes, no. of observations and RMS of residuals are listed for P_n and S_n phases, and also network magnitudes, which are the mean of all reported station magnitudes (P_n and S_n) for each event. Automatic network magnitudes (M_L) from NORSARs GBF system (Ringdal & Kværna, 1989) and the reference magnitudes (m_b) used to calibrate the magnitude scale (Ringdal & Kremenetskaya, 1999) are also shown. The two events marked in italic (1988-235 and 1995-162) could not be used as input to the inversion determining the attenuation relation for P_n and S_n.

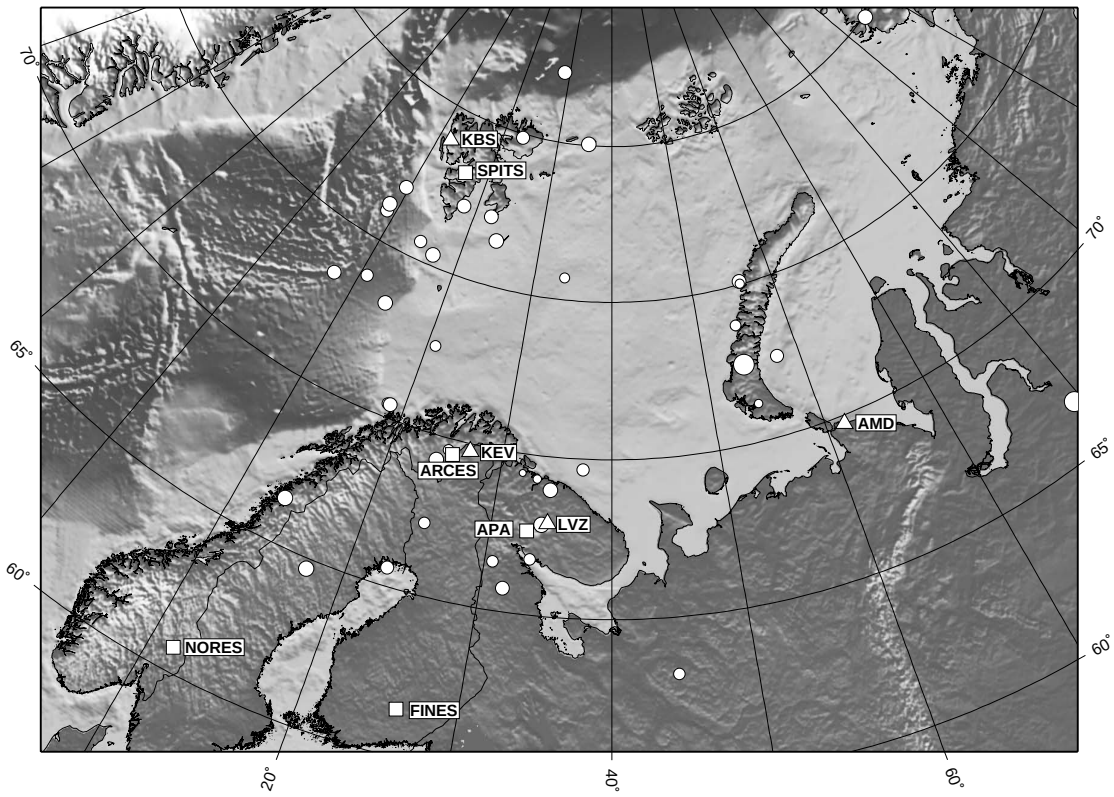

Fig. 6.2.1. Events (circles) and seismic stations used for deriving wave propagations characteristics of the Barents Sea and surrounding areas. Array stations are shown as squares, while 3C stations are shown as triangles. The event locations shown are after analysis and relocation using the BAREY model (Schweitzer and Kennett, 2002). The symbol size for the events are proportional to the network magnitudes in Table 6.2.3.

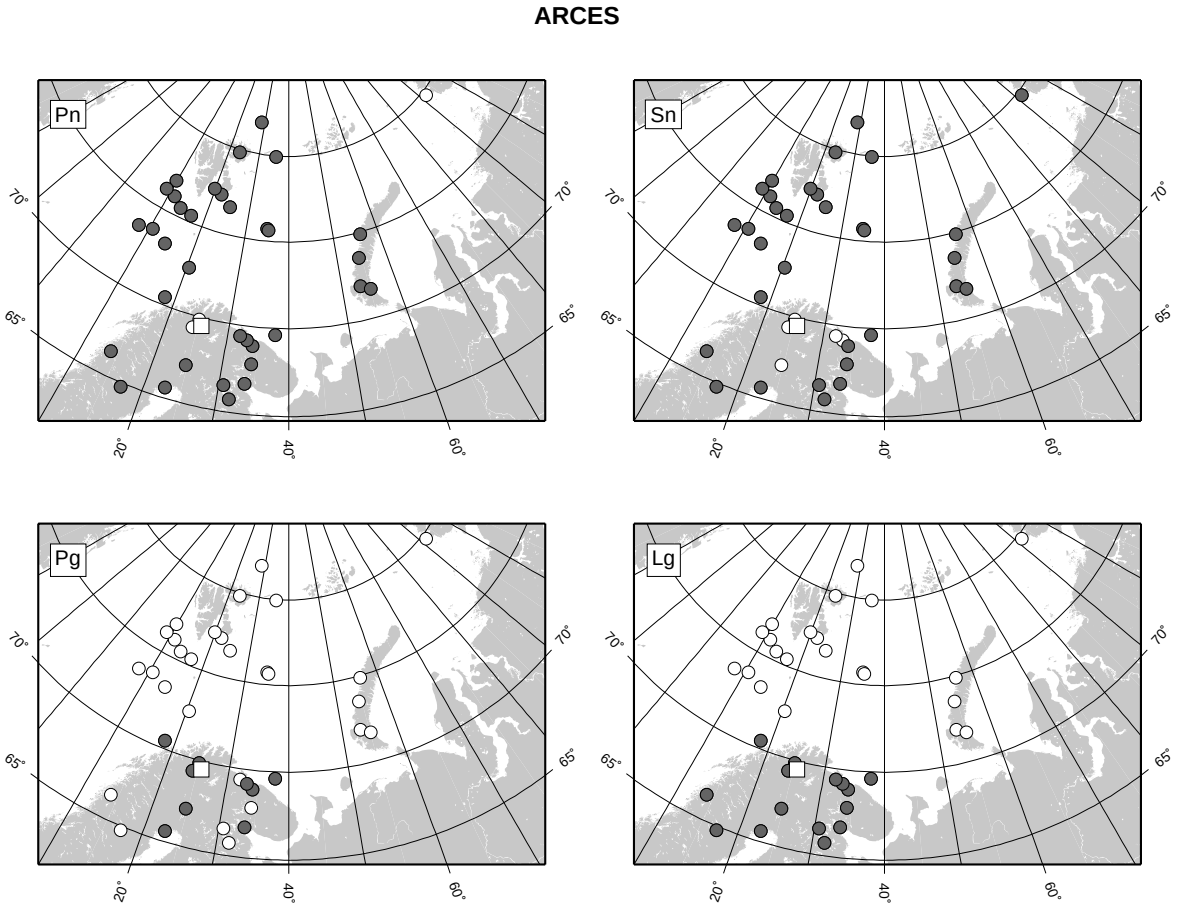

Fig. 6.2.2. Phase observations (dark circles) for P_n (upper left), P_g (lower left), S_n (upper right) and L_g (lower right) by the ARCES array (white square). The white circles represent events where the phase in question is not observed, but at least one other phase is observable.

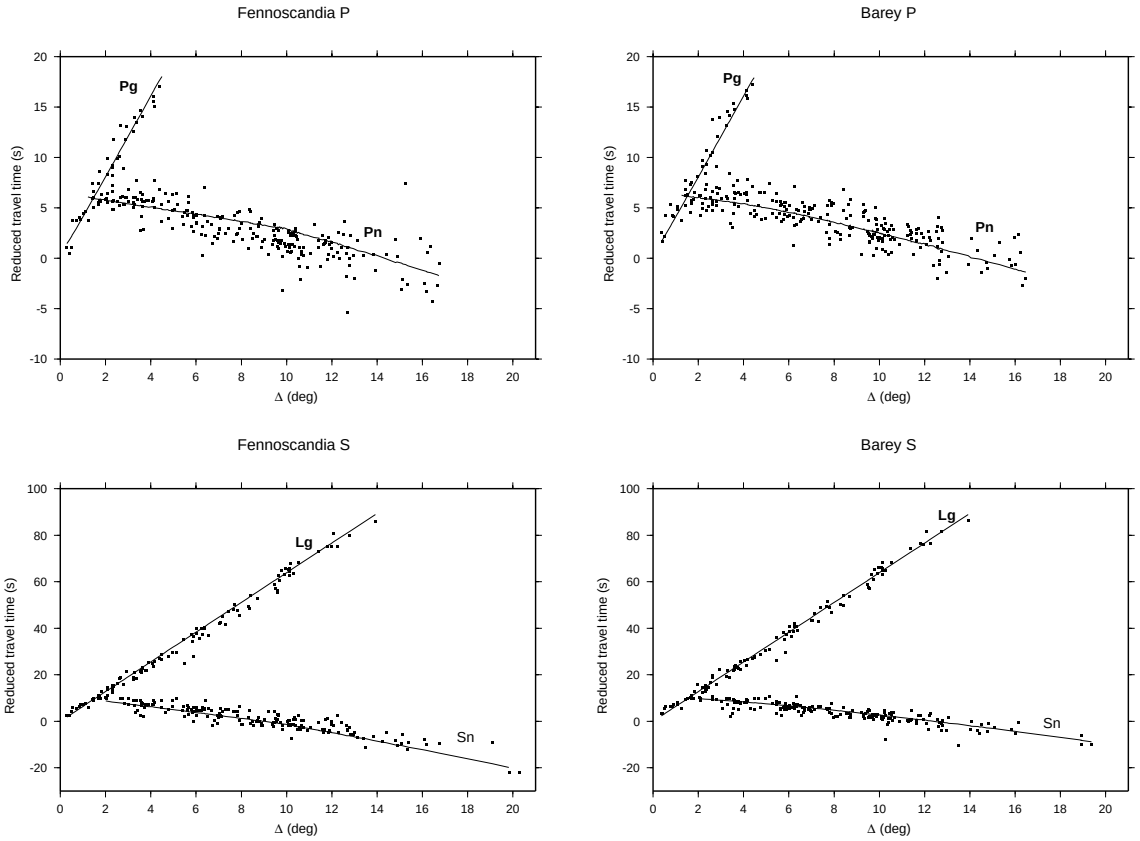

Fig. 6.2.3. Mykkeltveit and Ringdal (1981) and BAREY (right) (Schweitzer and Kennett, 2002) models. For the Fennoscandia model, P_n and L_g arrivals have mostly negative residuals while the S_n arrivals have positive residuals. The observations are distributed in a fairly symmetrical manner, and residuals are smaller (particularly for S phases) when the BAREY model is used. The travel times are reduced using 8.0 km/s for P and 4.5 km/s for S. Note that the vertical scales are different for the P and S plots.

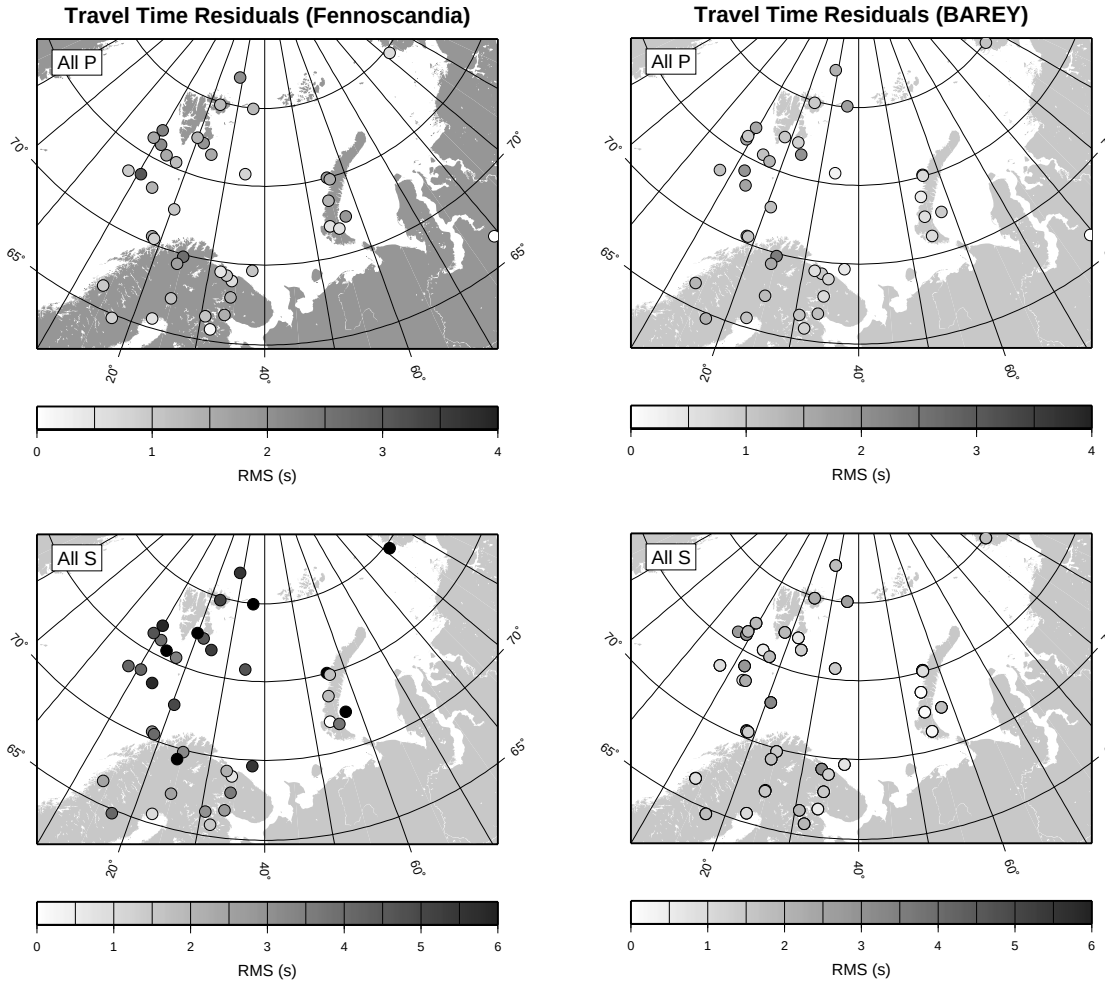

Fig. 6.2.4. RMS of travel time residuals for P (top) and S (bottom) phases for individual events located using the Fennoscandia (left) and BAREY (right) models, darker symbols indicate higher residuals. Events with larger residuals than 4.0 (P phases) or 6.0 (S phases) seconds are black.The residuals are generally smaller for locations using the BAREY model, in particular for the S phases.

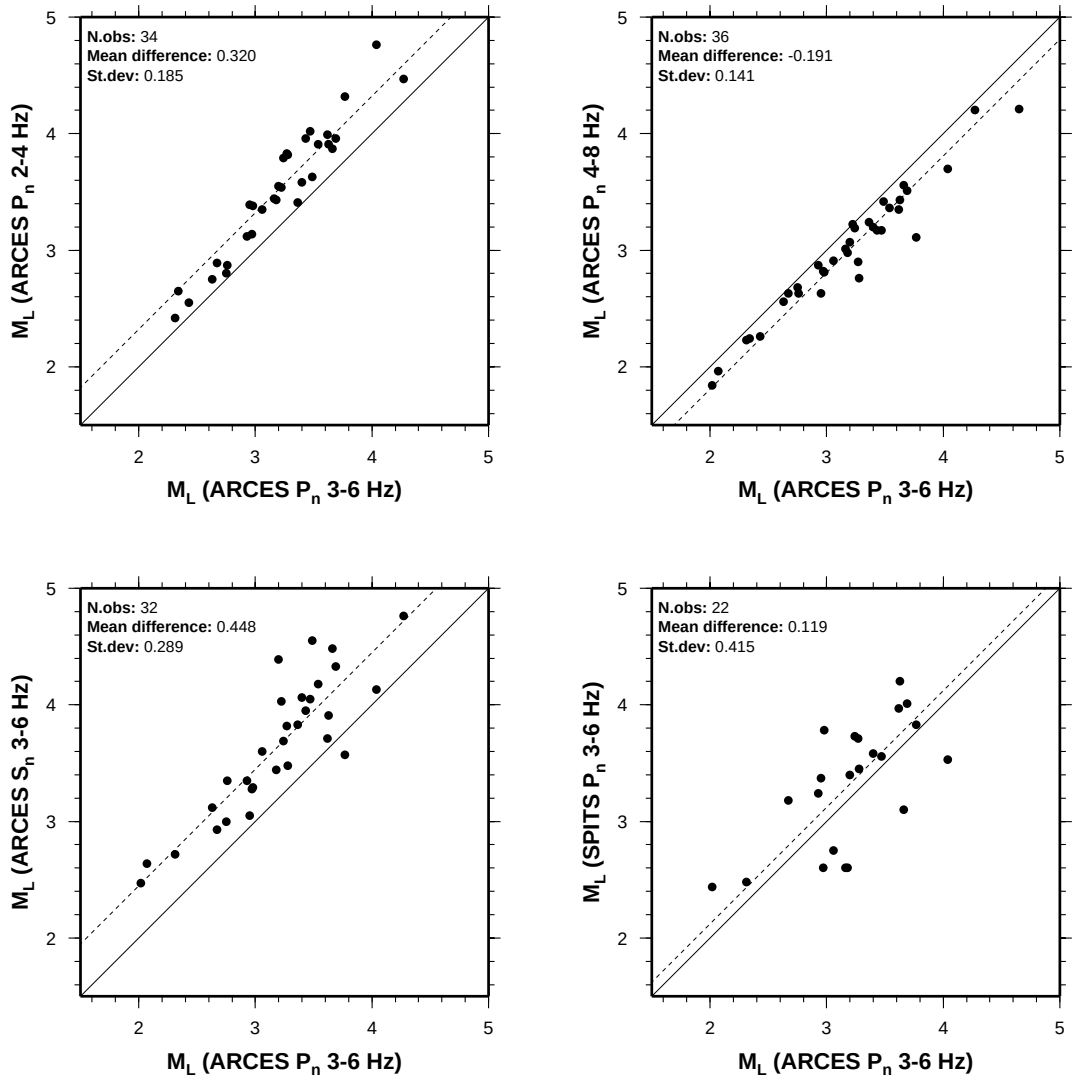

Fig. 6.2.5. Magnitudes calculated using the attenuation relation of Jenkins et al. (1998). Top: Comparison between different frequency bands at ARCES. Note the systematic trend towards lower magnitudes with increasing frequency. Lower left: Comparison between magnitudes calculated for P_n and S_n phases in the 3-6 Hz band at ARCES. The systematic offset is almost 0.5 magnitude units. Lower right: Comparison between P_n magnitudes in the 3-6 Hz band at ARCES and SPITS. The scatter (σ = 0.423) is quite large, with differences of up to a full magnitude unit for some events.

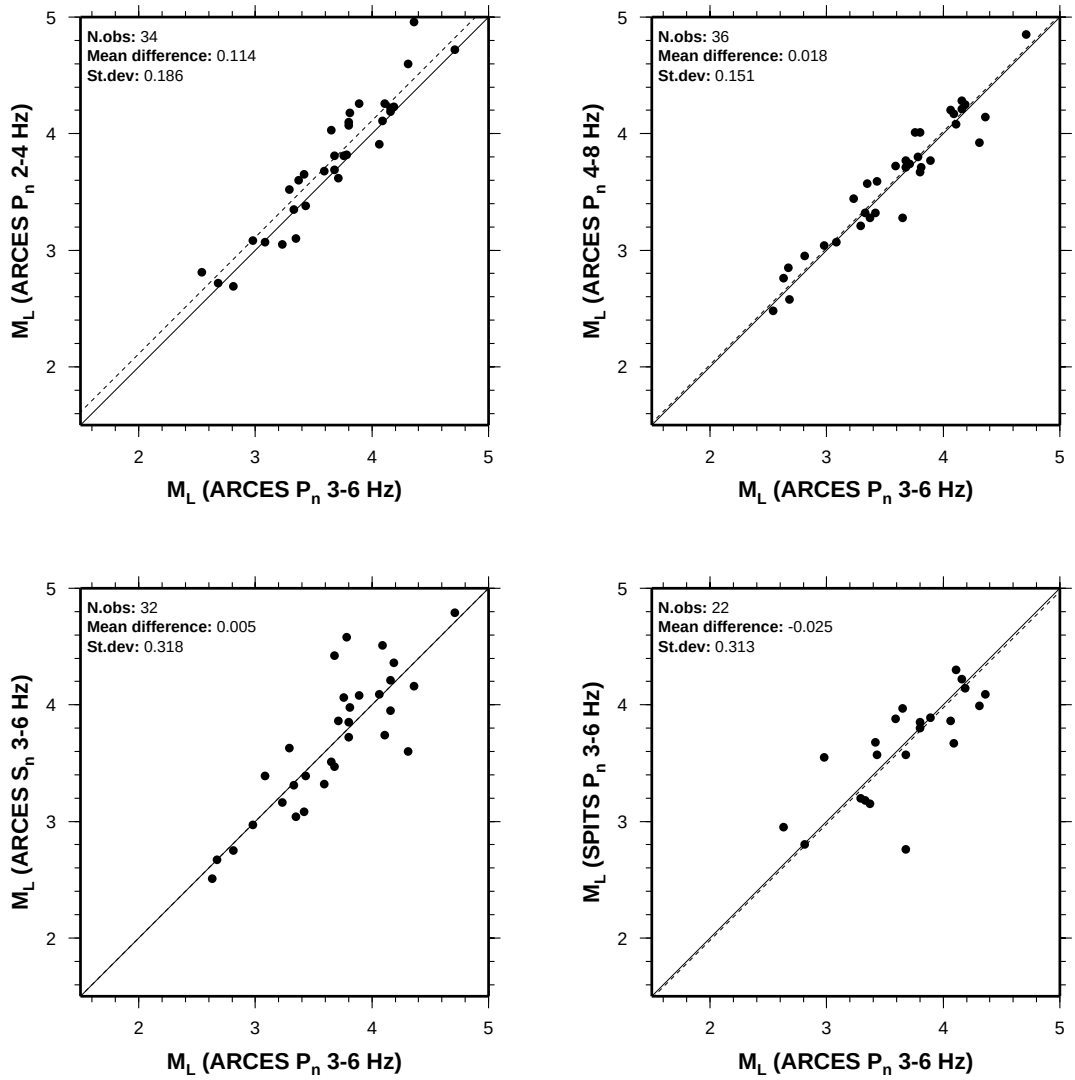

Fig. 6.2.6. Magnitudes calculated using the attenuation coefficients and station corrections from the inversion. Top: Comparison between different frequency bands at ARCES. The systematic frequency dependency as visible in Fig. 6.2.5 is significantly reduced. Lower left: Comparison between magnitudes calculated for P_n and S_n phases in the 3-6 Hz frequency band at ARCES. There is no obvious systematic offset, although the scatter is marginally increased compared to Fig. 6.2.5. Lower right: Comparison between P_n magnitudes in the 3-6 Hz frequency band at ARCES and SPITS. The average offset and scatter is reduced compared to Fig. 6.2.5.

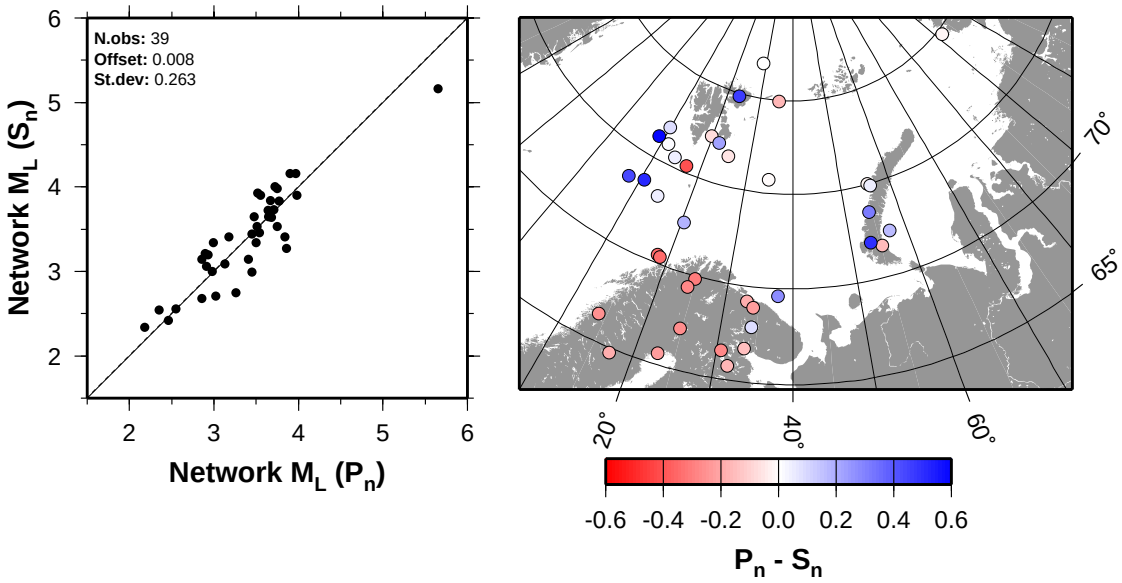

Fig. 6.2.7. Network event magnitude comparisons and maps of the geographical distribution of the magnitude differences for P_n vs. S_n. Note that S_n magnitudes are overestimated compared to P_n for events that have paths predominantly within the Baltic shield, while events with paths that cross the Barents Sea have larger P_n magnitudes compared to S_n.